

Spin-lattice coupling in magnetocaloric $\text{Gd}_5(\text{Ge,Si})_4$ alloys by *in situ* x-ray pair distribution analysis in magnetic field


Valeri Petkov ¹, Tadisetti D. Rao ^{1,2}, AM Milinda Abeykoon,³ Jorge R. Galeano-Cabral ⁴, and Kaya Wei⁴

¹Department of Physics, Central Michigan University, Mt. Pleasant, Michigan 48858, USA

²Department of Physics, GITAM (Deemed to be University), Visakhapatnam, Andhra Pradesh 530045, India

³Photon Sciences Division, Brookhaven National Laboratory, Upton, New York 11973, USA

⁴National High Magnetic Field Laboratory, Tallahassee, Florida 32310, USA

 (Received 20 April 2022; revised 5 September 2022; accepted 20 September 2022; published 13 October 2022)

Using *in situ* x-ray pair distribution analysis in magnetic field, we study the strong spin-lattice coupling in archetypal magnetocaloric $\text{Gd}_5(\text{Ge, Si})_4$ alloys manifested by the presence of a first order paramagnetic (PM)-to-ferromagnetic (FM) phase transition that can be triggered by either decreasing temperature in zero magnetic field or increasing magnetic field at constant temperature. We find that the coupling arises from the tendency of Gd-(Si,Ge) slabs in the alloys to reversibly slide against each other to both pack closely and couple ferromagnetically. We also find that, locally, the packing of slabs in FM phases induced by decreasing temperature in zero field is different from that in FM phases of the same chemical composition induced by increasing magnetic field isothermally, indicating that temperature and magnetic field are coupled but not necessarily equivalent control variables for triggering phase transitions in strongly correlated systems.

DOI: [10.1103/PhysRevMaterials.6.104407](https://doi.org/10.1103/PhysRevMaterials.6.104407)

I. INTRODUCTION

Rare earth-based systems exhibit strongly interacting lattice, electronic, and magnetic degrees of freedom, enabling better control over their remarkable properties explored for numerous practical applications [1–5]. A typical example is $\text{Gd}_5\text{Si}_x\text{Ge}_{4-x}$ alloys that exhibit colossal magnetoresistance, magnetostriction, and magnetocaloric effects, where magnetic refrigeration is achieved by harnessing concurrent changes in the magnetic and atomic configuration (crystal structure) entropy [6–8]. In particular, both end members and their mixtures are built of slabs of Gd and X atoms ($X = \text{Ge, Si}$) that are separated by layers of X atoms alone, as shown in Fig. 1. In the orthorhombic end member Gd_5Ge_4 , Ge atoms positioned between the slabs are too far apart to be considered bonded [Fig. 1(a)]. The alloy is paramagnetic (PM) at room temperature and upon cooling becomes an antiferromagnet at $T_N = 127$ K, where Gd-Ge slabs are ferromagnetic (FM) but anti-FM (AFM) coupled [9,10]. In the orthorhombic end member Gd_5Si_4 , Si atoms positioned between the slabs are close enough to be considered bonded, thus appearing as Si-Si dimers [Fig. 1(b)]. The alloy is paramagnetic at high temperature and becomes a usual ferromagnet at Curie temperature $T_C = 330$ K, where the FM Gd-Si slabs become ferromagnetically coupled [11,12]. In Si-rich ternary alloys ($2 \leq x \leq 4$), nonmetal X atoms between the slabs are bonded in dimers and the orthorhombic structure of the end member Gd_5Si_4 is preserved. The alloys are paramagnetic above room temperature and ferromagnetic at low temperature. In Ge-rich ternary alloys ($0 \leq x \leq 1$), no X - X dimers between the slabs exist and the orthorhombic structure of the end member Gd_5Ge_4 is preserved. On cooling, X - X dimers are formed, and the alloys

undergo a PM-to-FM phase transition. In the intermediate ternary $\text{Gd}_5\text{Si}_x\text{Ge}_{4-x}$ alloys ($0.8 \leq x \leq 2$), a large number of X - X dimers are broken at room temperature, reducing the average crystal symmetry to monoclinic. At low temperature, the broken X - X dimers and orthorhombic crystal symmetry are restored and FM order sets in. Notably, while for Si-rich phases the PM-to-FM phase transition is second order, it is first order for Ge-rich and intermediate alloys, involving unusually large shear movements of Ge- X slabs relative to one another [8,11,13–15]. Moreover, studies have found that the concurrent first order magnetic and structural phase transition in the alloys with $x \leq 2$ can also be induced by applying pressure or magnetic field isothermally [16–18]. For reference, the evolution of the crystal structure and magnetic state of $\text{Gd}_5\text{Si}_x\text{Ge}_{4-x}$ alloys with Si content and temperature is shown in Fig. 1(c).

It is assumed that indirect Ruderman-Kittel-Kasuya-Yosida (RKKY) interactions, which account for most magnetic phenomena observed in rare-earth-based systems [19–21], are behind the two-dimensional (2D) ferromagnetism of individual Gd- X slabs in $\text{Gd}_5\text{Si}_x\text{Ge}_{4-x}$ alloys. It is also assumed that the alloys become 3D ferromagnets only when X - X dimers appear between the slabs during the PM-to-FM transition, enabling Gd- X -Gd superexchange slab-slab interactions [6,8,13,19]. While the first assumption is generally accepted, the second assumption remains controversial. [6,20–22]. This is because it leaves the question of how magnetic field triggers a PM-to-FM transition in a system where the magnetic rare-earth species lack orbital momentum unanswered. To address the controversy, we study the evolution of the crystal structure of representative $\text{Gd}_5\text{Si}_x\text{Ge}_{4-x}$ alloys [$x = 0.2, 0.7, \text{ and } 1.7$; see the phase diagram in Fig. 1(c)] over a broad range of

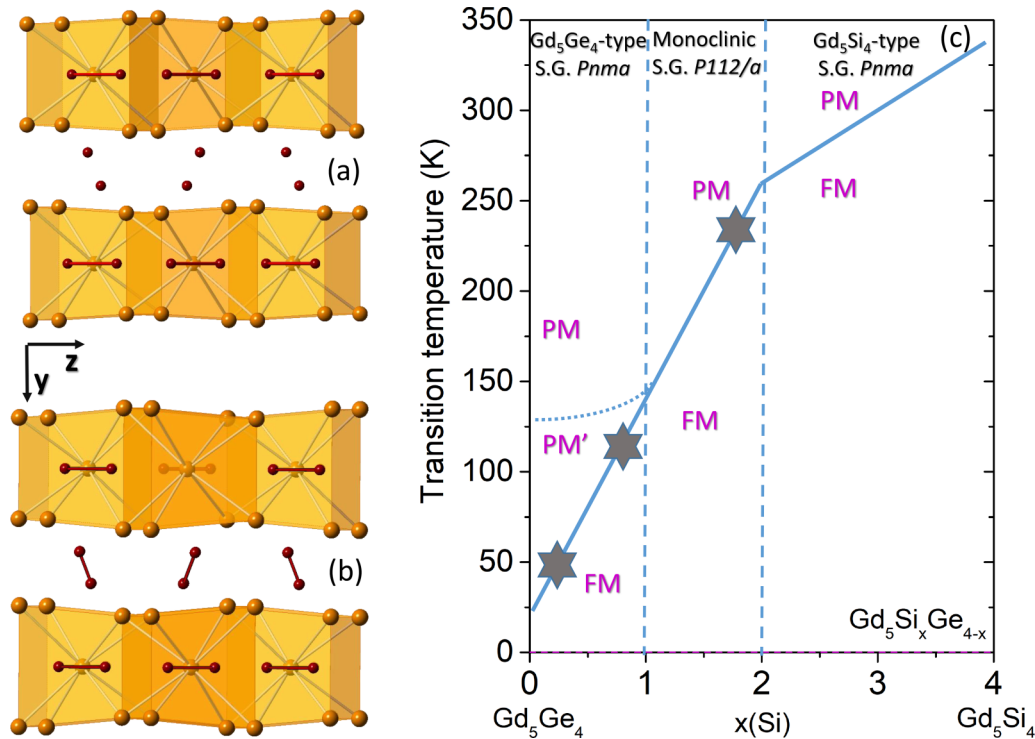


FIG. 1. Left: Fragments from the orthorhombic crystal structure of (a) Gd_5Ge_4 and (b) Gd_5Si_4 alloys featuring slabs of Gd (brown) and nonmetal (red) atoms separated by layers of nonmetal atoms alone, which are bonded (brown line) in the case of the latter. Directions of the orthorhombic lattice are given as arrows. Right: Magnetic phase diagram for $Gd_5Si_xGe_{4-x}$ alloys. Blue solid line separates paramagnetic (PM) and ferromagnetic (FM) phases. Vertical broken lines delineate Ge-rich ($0 \leq x \leq 1$), Si-rich ($2 \leq x \leq 4$), and intermediate ($1 \leq x \leq 2$) alloys, exhibiting an orthorhombic Gd_5Ge_4 , orthorhombic Gd_5Si_4 , and monoclinic-type structure in their PM state, respectively. The average crystal structure of all alloys in their FM state is considered to be of the orthorhombic, Gd_5Si_4 type. The Ge-rich alloys also exhibit a phase transition between two paramagnetic phases, PM and PM' (dotted blue line), where the latter exhibits a short-range antiferromagnetic-like order. The alloy compositions studied here are marked with stars.

magnetic fields and temperatures, including the PM-to-FM phase transition. Using x-ray atomic pair distribution function (PDF) analysis, we show that, regardless of whether induced by decreasing temperature or applying magnetic field, the transition dramatically modifies the mutual arrangement of nearby Gd atoms, thus modifying the character of slab-slab exchange interactions. This may not come as a big surprise because the arrangement of nearby Gd atoms in the Gd_5Si_5 - and Gd_5Ge_4 -type structures is considerably different [see Fig. 2(a)]. We also show that, likely due to the presence of distinct Gd-Ge and Gd-Si bonds, the ternary alloys exhibit considerable lattice distortions, rendering their local structure monoclinic in the nominally orthorhombic FM state. Moreover, the distortions appear dependent on whether the PM/FM phase boundary is crossed by decreasing temperature or increasing magnetic field, providing evidence that temperature and magnetic field are coupled but not necessarily equivalent control variables for triggering phase transitions in strongly correlated systems in general and $Gd_5Si_xGe_{4-x}$ alloys in particular.

II. EXPERIMENT

Sample preparation and properties characterization. Samples were prepared by arc melting of Gd (99.9%, Alfa Aesar), Ge (99.999%, Alfa Aesar) and Si (99.999% + %, Alfa Aesar)

lumps intermixed in due proportions. All samples were melted five times and turned over each time to improve homogeneity. For the annealing process, the samples were sealed under vacuum in quartz tubes, heated to 1545 K, and held at that temperature for 72 h. In line with the findings of prior studies, in house x-ray diffraction (XRD) experiments showed that, at room temperature, $Gd_5Si_{0.2}Ge_{3.8}$ and $Gd_5Si_{0.7}Ge_{3.3}$ alloys are orthorhombic while the average crystal symmetry of $Gd_5Si_{1.7}Ge_{2.3}$ alloy is monoclinic. Magnetic properties were studied on a physical property measuring system (PPMS) from Quantum Design. Results are shown in Figs. 2(c)–2(f). As can be seen in Fig. 2(c), the alloys undergo a sharp PM-to-FM transition with decreasing temperature. In line with the findings of previous studies [6,12,17,23,24], the transition (Curie) temperature, T_C , increases with Si content. Data in Figs. 2(d)–2(f) also show that FM order can be induced by applying an external magnetic field in the order of 5 T at a fixed temperature slightly above T_C .

Synchrotron radiation studies. Synchrotron high-energy XRD experiments were conducted at the beamline 28-ID-1 (PDF) at the National Synchrotron Light Source-II, Brookhaven National Laboratory using x rays with energy of 74.46 keV ($\lambda = 0.1665 \text{ \AA}$). Powder samples were sealed in Kapton tubes and positioned inside a liquid He cryostat used to control their temperature. X-ray diffraction data were obtained in transmission geometry, and scattered intensities

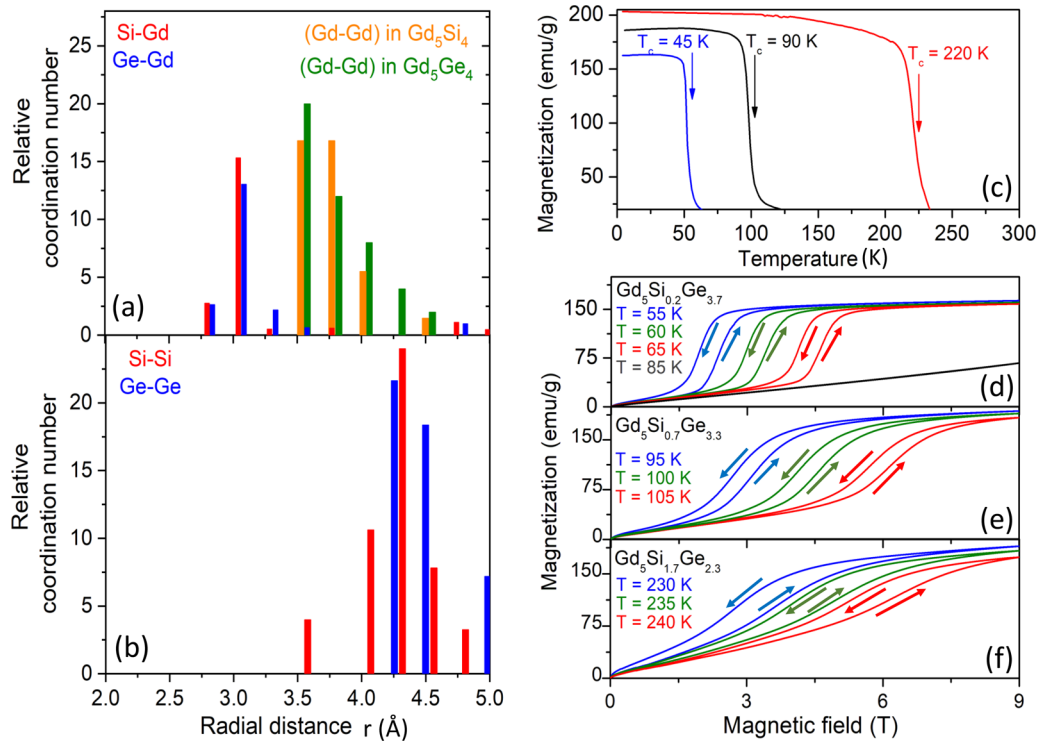


FIG. 2. (a),(b) Atomic pair correlations in orthorhombic Gd_5Ge_4 and Gd_5Si_4 alloys. Si-involving atomic pair distances (red bars) are shorter than the respective Ge-involving distances (blue bars) because Si atoms are smaller in size in comparison to Ge atoms. Notably, the distribution of Gd-Gd atomic pairs in these alloys appears different [orange vs green bars in (a)]. (c) Temperature evolution of magnetization for $\text{Gd}_5\text{Si}_{0.2}\text{Ge}_{3.8}$ (blue), $\text{Gd}_5\text{Si}_{0.7}\text{Ge}_3$ (black), and $\text{Gd}_5\text{Si}_{1.7}\text{Ge}_{2.3}$ (red) alloys measured in magnetic field of 0.1 T. Upon cooling the alloys, the magnetization exhibits a sharp upturn at, respectively, $T_c = 45$, 90, and 220 K, characteristic to a first order PM-to-FM phase transition. (d)–(f) Field evolution of the magnetization for $\text{Gd}_5\text{Si}_x\text{Ge}_{4-x}$ alloys measured at a few temperatures just above the respective T_c . Data indicate the presence of a field induced (metamagnetic) PM-to-FM phase transition, including the presence of magnetic hysteresis. No such transition can be induced, i.e., magnetization vs field dependence remains a straight line, when the measurement temperature is considerably above T_c , e.g., a measurement temperature of 85 K for $\text{Gd}_5\text{Si}_{0.2}\text{Ge}_{3.8}$ alloy [black line in (d)] vs $T_c = 45$ K. Arrows in (d)–(f) indicate the ascending and descending branches of the hysteresis curves.

were collected using an amorphous silicon PerkinElmer area detector. For each of the samples, data were taken over a temperature range from 300 K down to 5 K, in steps of 5 K. Two data sets were obtained at each temperature point. One of the data sets was obtained with the detector positioned 1000 mm away from the sample to achieve high resolution in reciprocal space necessary for the Rietveld analysis described below. The other data set was obtained with the detector positioned 204 mm away from the sample to reach high wave vectors q ($q_{\text{max}} = 28 \text{ \AA}^{-1}$ in the current experiment) necessary to obtain high real space resolution atomic PDFs. The PDFs were derived from the XRD data following a well-established protocol [25]. Experimental XRD patterns and atomic PDFs obtained at different temperatures are summarized in Fig. 3 in terms of intensity color maps. The patterns and PDFs are seen to undergo sharp changes at a temperature where, according to the independently collected magnetic data [Fig. 2(c)], a PM-to-FM transition takes place, confirming the presence of concurrent structural and magnetic phase transitions in $\text{Gd}_5\text{Si}_x\text{Ge}_{4-x}$ alloys. High-energy XRD data were also obtained at 329 K, i.e., slightly above T_c , while applying an external magnetic field with a strength of up to 5 T. Because of experimental constraints related to the combined use of an electromagnet and cryostat, this time x rays with energy of

116.63 keV ($\lambda = 0.1063 \text{ \AA}$) were used. Atomic PDFs were derived from the diffraction data collected in magnetic field, summarized in Fig. 2(d). As can be seen in the figure, the PDFs exhibit significant hysteresis effects.

III. CRYSTAL STRUCTURE ANALYSIS

Average crystal structure. To reveal the temperature evolution of the average crystal structure, high q -resolution XRD data were subjected to Rietveld analysis using the software GSAS II [26]. Representative Rietveld fits and refined lattice parameters are summarized in Figs. 4 and 5, respectively. Results of the Rietveld analysis confirm that the average crystal structure of both PM and FM phases of Ge-rich ($\text{Gd}_5\text{Si}_{0.2}\text{Ge}_{3.8}$ and $\text{Gd}_5\text{Si}_{0.7}\text{Ge}_{3.3}$) alloys is orthorhombic (space group $Pnma$). For the intermediate $\text{Gd}_5\text{Si}_{1.7}\text{Ge}_{2.3}$ alloy, the Rietveld analysis found that, on average, the room temperature PM phase is monoclinic (space group $P112_1/a$) and the low-temperature FM phase appears orthorhombic (space group $Pnma$). The results are in line with the findings of prior studies [6,8,16,18]. Notably, it was found that for all alloys, the PM-to-FM phase transition is accompanied by a significant change (2%) in the a lattice parameter and moderate changes (less than 0.5%) in the b and c lattice parameters.

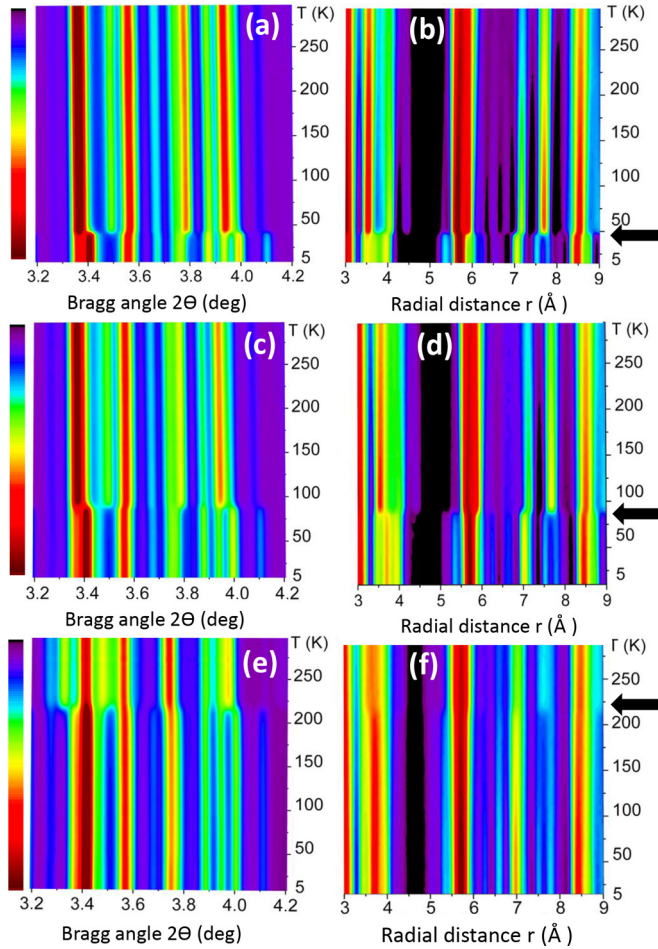


FIG. 3. Synchrotron XRD (left) and atomic PDF (right) intensity color maps for $\text{Gd}_5\text{Si}_{0.2}\text{Ge}_{3.8}$ (a),(b), $\text{Gd}_5\text{Si}_{0.7}\text{Ge}_{3.3}$ (c),(d), and $\text{Gd}_5\text{Si}_{1.7}\text{Ge}_{2.3}$ (e),(f) alloys. For each of the alloys, data indicate the presence of a sharp structural phase transition at a temperature (black horizontal arrows) where they also undergo a first order PM-to-FM transition [see magnetization data in Fig. 2(c)]. Note that the intensity of XRD and PDF features increases as their color changes from blue towards dark red. The increase is at a constant rate, as indicated by the color bar on the left of each plot.

The significant change in the a lattice parameter reflects the fact that, during the transition, Gd-X slabs slide against each other in a direction parallel to the a axis of the crystal lattice. In addition, for all alloys and in line with the findings of prior studies [6,7,16,18], the volume of the crystallographic unit cell was found to sharply diminish when 3D FM order sets in. The reason is the tendency of Gd-X slabs in FM phases to pack in a manner similar to that in Gd_5Si_4 , whose unit cell volume is smaller than that in ternary $\text{Gd}_5(\text{Si}, \text{Ge})_4$ alloys. Rietveld analysis, however, is insensitive to likely local structural distortions in $\text{Gd}_5\text{Si}_x\text{Ge}_{4-x}$ alloys resulting from the presence of distinct Si and Ge atoms in the same Wyckoff positions.

Local crystal structure. To investigate the distortions, we performed atomic PDF analysis that has proven sensitive to both the average crystal structure and local deviations from it

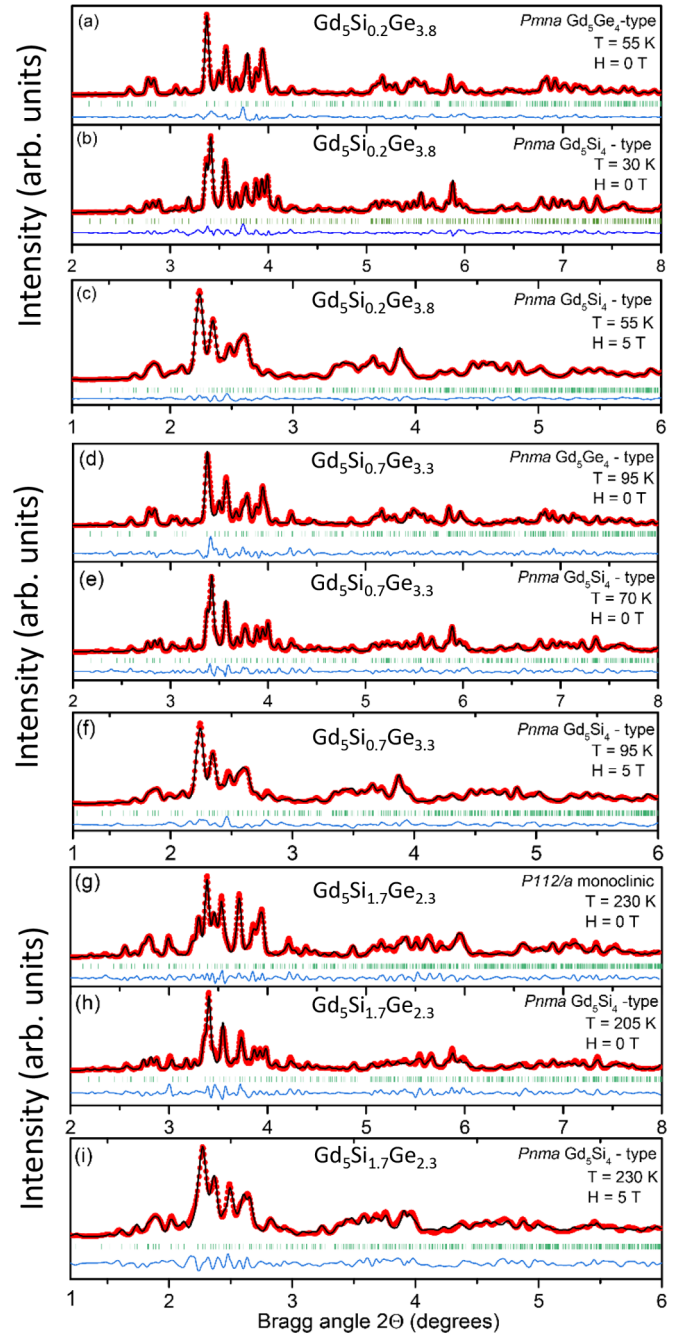


FIG. 4. Rietveld fits (black) to XRD patterns (red) for (a)–(c) $\text{Gd}_5\text{Si}_{0.2}\text{Ge}_{3.8}$, (d)–(f) $\text{Gd}_5\text{Si}_{0.7}\text{Ge}_{3.3}$, and (g)–(i) $\text{Gd}_5\text{Si}_{1.7}\text{Ge}_{2.3}$ alloys obtained at a temperature (a),(d),(g) above and (b),(d),(h) below the respective T_C in zero magnetic ($H = 0$) field. Fits to XRD data (c),(f),(i) taken in magnetic field with a strength of 5 T at a temperature just above T_C [same as the temperature in (a),(d),(g)] are also shown. The type of refined structure model is shown for each data set. The residual difference (blue) is shifted for clarity. The XRD patterns in magnetic field (c),(f),(i) are taken using x rays with a wavelength shorter ($\lambda = 0.1063 \text{ \AA}$) than that ($\lambda = 0.1665 \text{ \AA}$) used to collect the XRD patterns in zero field. Accordingly, the former appear compressed toward lower Bragg angles and with a diminished resolution in comparison to the latter. The goodness-of-fit indicator R_{wp} for all fits is in the order of 6–9%.

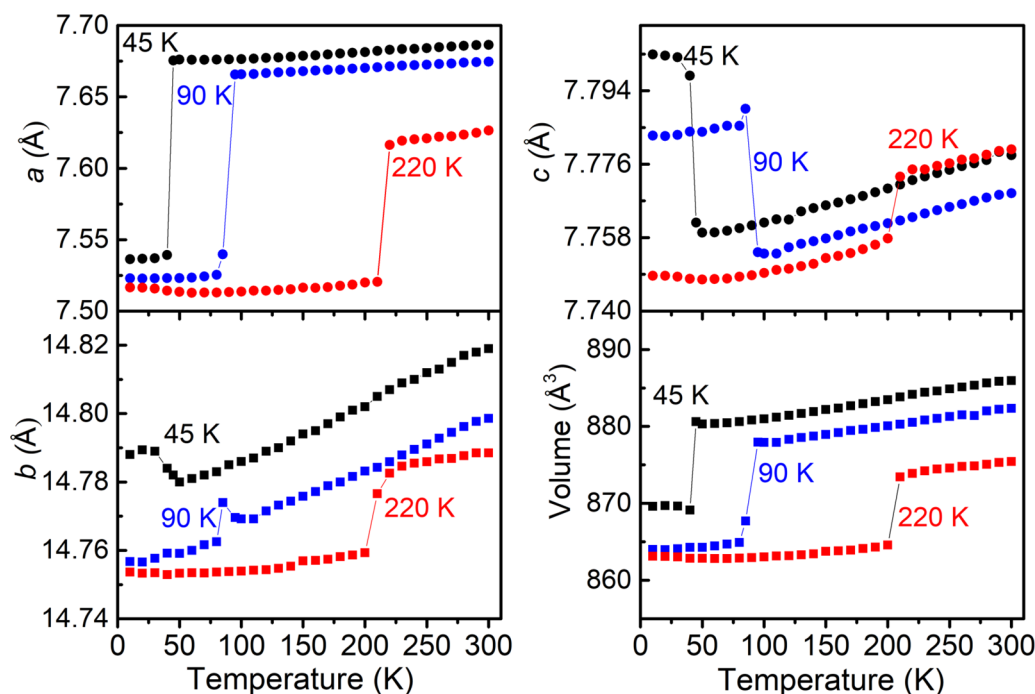


FIG. 5. Temperature evolution of the lattice parameters a , b , and c for $\text{Gd}_5\text{Si}_{0.2}\text{Ge}_{3.8}$ (black), $\text{Gd}_5\text{Si}_{0.7}\text{Ge}_{3.3}$ (blue), and $\text{Gd}_5\text{Si}_{1.7}\text{Ge}_{2.3}$ (red) alloys obtained by Rietveld analysis of XRD data. Data for the unit cell volume are also shown. It is seen to diminish sharply at the PM-to-FM transition temperature T_C , which is given for each data set. The lattice parameters are also seen to exhibit a sharp change at T_C .

[27,28]. The low- r part of experimental atomic PDFs obtained at a few different temperature points just above and below the respective T_C in zero field is shown in Fig. 6. Also shown in the figure are atomic PDFs obtained at a preselected temperature just above T_C while gradually increasing the external magnetic field from 0 to 5 T. As shown by our magnetic data [see Figs. 2(d)–2(f)], at that temperature, the alloys undergo a first order metamagnetic phase transition, where a sharp increase in the magnetization is observed when the applied external field reaches a critical value. The transition is reversible and, similarly to the temperature induced PM-to-FM transition, exhibits significant hysteresis effects (see Figs. S2–S4 in the Supplemental Material [29]).

In the end members of $\text{Gd}_5\text{Si}_x\text{Ge}_{4-x}$ alloys, near neighbor X - X and Gd - X distances appear in the range from about 2.4 to 2.8 Å and in the range from about 2.9 to 3.1 Å, respectively. Most X - X distances, however, appear above 4 Å. On the other hand, the distances between near neighbor Gd atoms appear in the range 3.5–4 Å [see Figs. 2(a) and 2(b)]. As can be seen in Fig. 6, PDF peaks positioned between 3.5 and 4 Å, which largely reflect Gd - Gd distances, change markedly in position and/or intensity when the PM/FM phase boundary is crossed by either decreasing temperature or increasing magnetic field. The results indicate that nearby Gd atoms markedly rearrange with respect to each other during the PM-to-FM transition. By contrast, the PDF peak at about 3.0 Å, which largely reflects Gd - X distances, does not change much either in position and/or intensity, reflecting the fact that Gd - X slabs in both PM and FM phases are virtually the same. Comparison between an experimental PDF for a FM phase induced by decreasing temperature in zero field with that for a chemically

equivalent FM phase induced by increasing the magnetic field at constant temperature, e.g., the PDF for $\text{Gd}_5\text{Si}_{0.7}\text{Ge}_{3.3}$ obtained at 70 K in zero magnetic field with that for the same sample obtained at 95 K in magnetic field of 5 T [follow blue curves in Figs. 6(b), 6(d), and 6(f), and Fig. S6 [29]], reveals the presence of significant differences between the two. The differences indicate that the local atomic structure of such phases is not exactly the same, as discussed further below.

To determine the level of differences, the atomic PDFs in Fig. 6 were fit with structure models for orthorhombic Gd_5Ge_4 [Fig. 1(a)], orthorhombic Gd_5Si_4 [Fig. 1(b)], and a monoclinic phase (space group $P112_1/a$) found useful in describing intermediate PM $\text{Gd}_5\text{Si}_x\text{Ge}_{4-x}$ alloys [8]. The fits were done with the help of software PDFGUI [30]. Results from representative fits are shown in Fig. 7. Similarly to the average crystal structure determined by Rietveld analysis [Figs. 4(a) and 4(d)], the local structure of PM $\text{Gd}_5\text{Si}_{0.2}\text{Ge}_{3.8}$ and $\text{Gd}_5\text{Si}_{0.7}\text{Ge}_{3.3}$ phases is found to be of the orthorhombic Gd_5Ge_4 type [Figs. 7(a) and 7(d)]. Contrary to the findings of Rietveld analysis [Figs. 4(b), 4(c), 4(e), and 4(f)], the PDF analysis shows that the local structure of low-temperature FM $\text{Gd}_5\text{Si}_{0.2}\text{Ge}_{3.8}$ and $\text{Gd}_5\text{Si}_{0.7}\text{Ge}_{3.3}$ phases is monoclinic and not orthorhombic [Figs. 7(b), 7(c), 7(e), and 7(f)]. In the case of room temperature PM $\text{Gd}_5\text{Si}_{1.7}\text{Ge}_{2.3}$ phase, both the average [Fig. 4(g)] and local [Fig. 7(g)] crystal structure appear monoclinic. However, contrary to the findings of Rietveld analysis [Figs. 4(h) and 4(i)], the PDF analysis shows that the local structure of the low-temperature FM $\text{Gd}_5\text{Si}_{1.7}\text{Ge}_{2.3}$ phase retains the monoclinic symmetry of the higher-temperature PM phase [Figs. 7(h) and 7(i)]. For comparison, fits to PDF

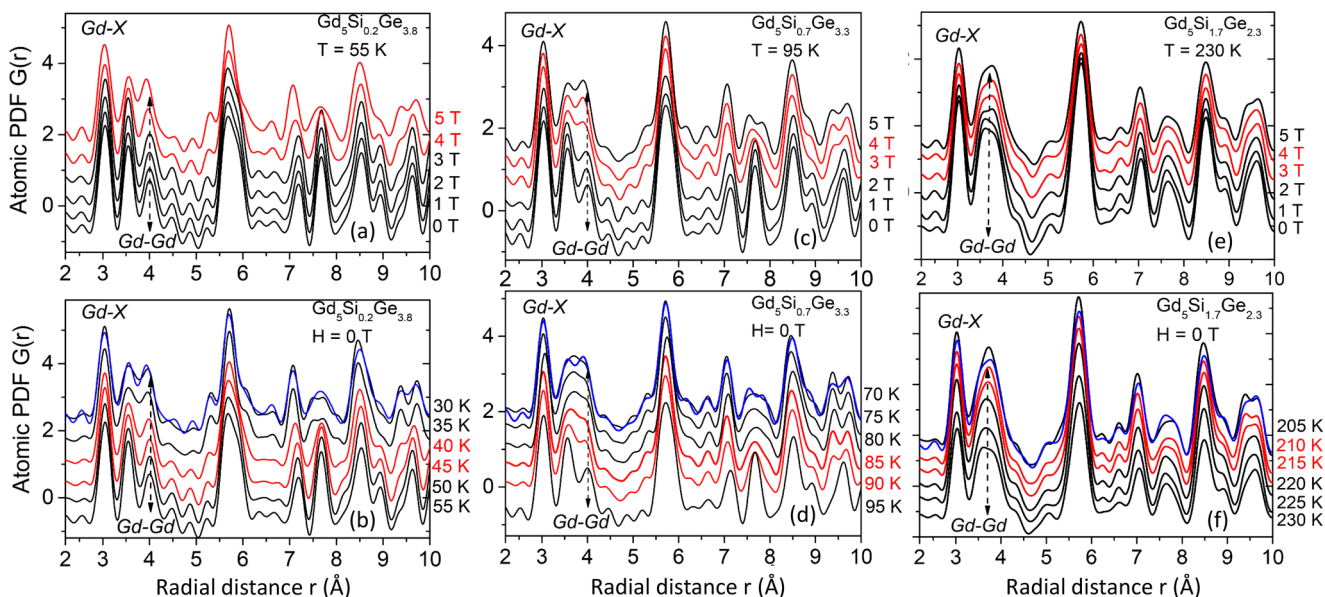


FIG. 6. (lower panels) Low- r part of experimental atomic PDFs for $Gd_5Si_5Ge_{4-x}$ alloys obtained at different temperature points close to the PM-to-FM phase transition temperature T_C , in zero ($H = 0$) magnetic field. Upper panels: Low- r part of experimental atomic PDFs for the same samples obtained at a fixed temperature just above T_C this time in nonzero magnetic field while increasing it from 0 to 5 T in steps of 1 T. The particular temperature and applied magnetic field are given for each data set. PDFs obtained in the immediate vicinity of T_C /critical magnetic field at which the transition takes place are highlighted in red. For each sample, the PDF obtained at 5 T [top curve in (a),(c),(e)] is superimposed (blue line) on the PDF for the same sample obtained in zero field but at a lower temperature [top curve in (b),(d),(f)], where the sample also is in a ferromagnetic state. The two PDFs differ significantly (also see Fig. S6 [29]). Note that the PDFs are particularly sensitive to Gd-involving atomic-pair correlations because Gd atoms scatter x rays much stronger than nonmetal Si and Ge atoms do. The PDF peak at about 3 Å reflects first neighbor Gd-X atomic correlations ($X = Si, Ge$) while the PDF peaks positioned between 3.5 and 4 Å largely reflect near neighbor Gd-Gd distances [see Figs. 2(a) and 2(b)]. The peaks are seen to undergo a marked evolution with decreasing temperature/increasing magnetic field.

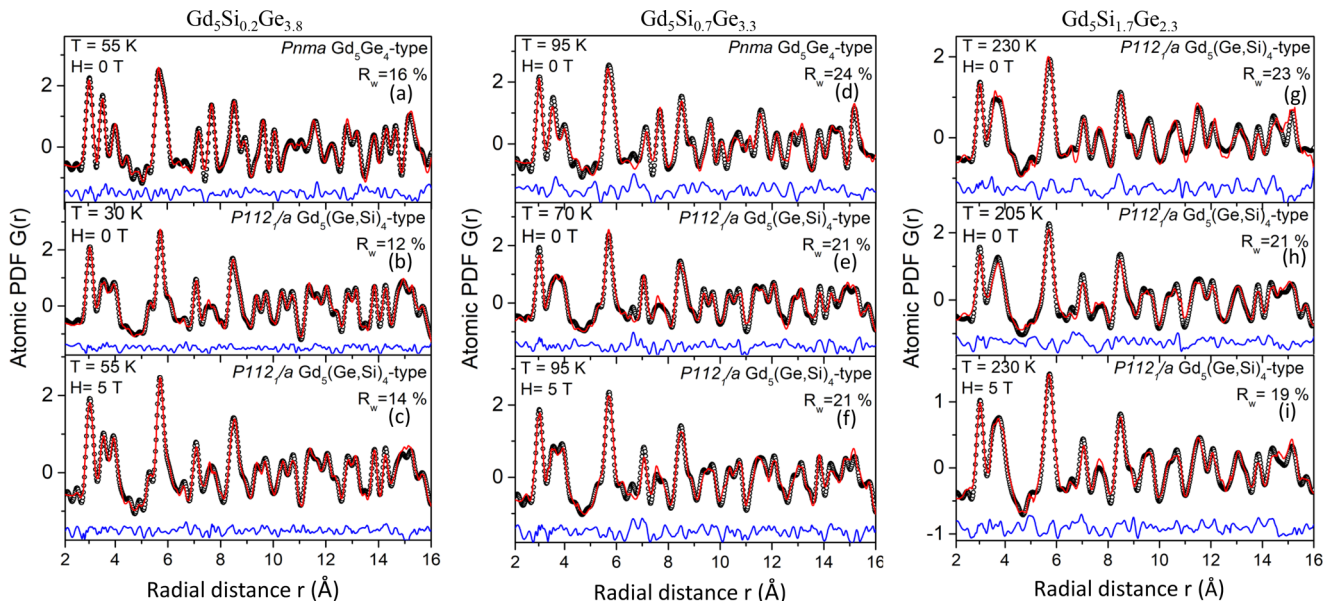


FIG. 7. Fits (red line) to experimental atomic PDFs (symbols) for $Gd_5Si_5Ge_{4-x}$ alloys obtained just above (a),(d),(g) and below (b),(e),(h) the respective T_C in zero magnetic field ($H = 0$ T). Also shown (c),(f),(i) are fits (red line) to experimental PDFs (symbols) obtained at temperature just above the respective T_C , this time in external magnetic field of 5 T. The field is capable of inducing FM order, as data in Figs. 2(d)–2(f) and S5 [29] show. The structure model type, goodness-of-fit factor R_w , and residual difference (blue line) are given for each data set. Note that attempts to fit the experimental PDF data in (b), (e), and (h) with an orthorhombic (space group $Pnma$) models are less successful (see Fig. 8) than the monoclinic fits shown here are.

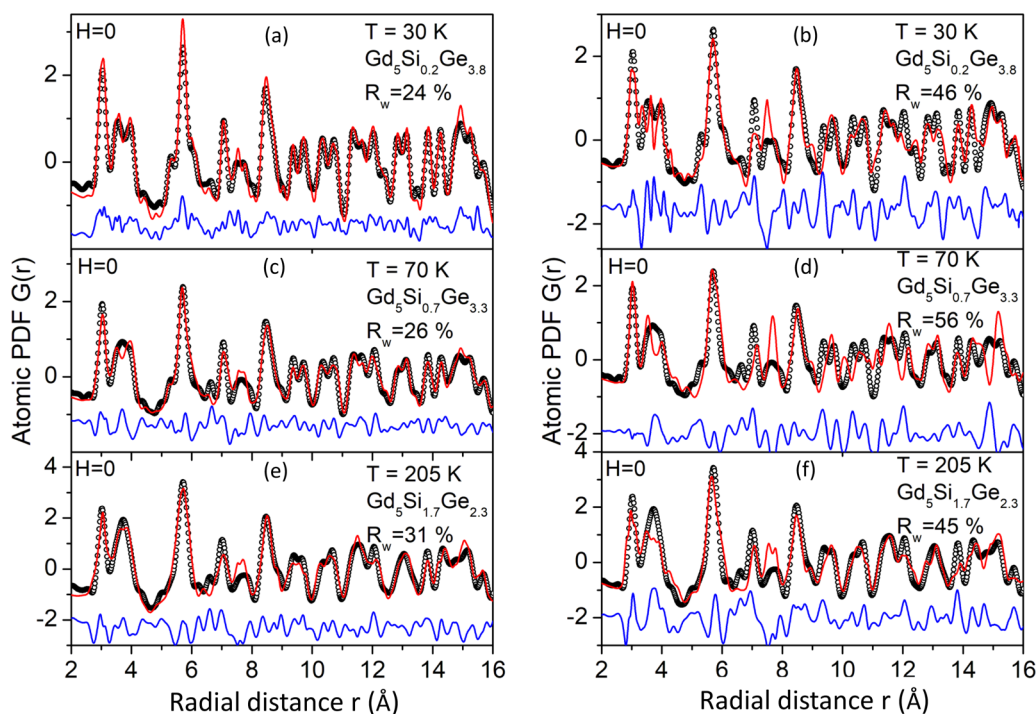


FIG. 8. Fits (red) to the experimental (symbols) atomic PDFs for (a),(b) $\text{Gd}_5\text{Si}_{0.2}\text{Ge}_{3.8}$, (c),(d) $\text{Gd}_5\text{Si}_{0.7}\text{Ge}_{3.3}$, and (e),(f) $\text{Gd}_5\text{Si}_{1.7}\text{Ge}_{2.3}$ alloys obtained in zero external magnetic field at temperature below the respective T_C [same as the PDFs in Figs. 7(b), 7(e), and 7(h)]. The fits in (a),(c),(e) are based on the orthorhombic (space group $Pnma$) structure of Gd_5Si_4 and those in (b),(d),(f) are based on the orthorhombic (space group $Pnma$) structure of Gd_5Ge_4 . They are inferior to the respective fits in Figs. 7(b), 7(e), and 7(h) based on a monoclinic (space group $P112_1/a$) structure. The residual difference (blue) is shifted downward by subtracting a constant for clarity.

data for low-temperature FM alloys based on orthorhombic Gd_5Si_4 - and Gd_5Ge_4 -type models are shown in Fig. 8. The fits are clearly inferior to those based on the monoclinic model [Figs. 7(b), 7(e), and 7(h)].

Local vs average crystal structure in $\text{Gd}_5\text{Si}_x\text{Ge}_{4-x}$ alloys. The picture emerging from our studies is as follows: The local and average crystal structure in the room temperature PM phases of as synthesized $\text{Gd}_5\text{Si}_x\text{Ge}_{4-x}$ alloys ($x = 0.2, 0.7, 1.7$) appear to be the same. The local and average crystal structure in the low-temperature FM phases of the alloys are, however, not the same. The likely reason is the emergence of lattice distortions/strain during the transition, where Gd-X slabs slide with respect to one another, and distinct Si-Si and Ge-Ge dimers are formed. The distortions may be expected to be larger in the intermediate $\text{Gd}_5\text{Si}_x\text{Ge}_{4-x}$ alloys in comparison to Ge-rich and Si-rich alloys and, furthermore, serve as a bridge linking their monoclinic PM and nominally orthorhombic but locally monoclinic FM phases. The emergence of local lattice distortions is consistent with the observed initial increase in the resistivity of the latter in comparison to the former [31,32]. Not only are the local and average structure of studied FM phases not the same, but also the local atomic structure of FM phases induced by crossing the PM/FM phase boundary by decreasing temperature [Figs. 7(b), 7(e), and 7(h)] is different from that of chemically identical FM phases induced by increasing magnetic field isothermally [Figs. 7(c), 7(f), and 7(i)]. The difference is well manifested by PDF fit derived lattice parameters for the alloys summarized in Table I. Likely, the difference appears because temperature changes directly affect both the

metal Gd and nonmetal Si/Ge sublattices of $\text{Gd}_5\text{Si}_x\text{Ge}_{4-x}$ alloys whereas changes in the external magnetic field primarily affect the “magnetic” Gd sublattice, as discussed below.

TABLE I. PDF refined lattice parameters for ferromagnetic $\text{Gd}_5\text{Si}_x\text{Ge}_{4-x}$ alloys at a temperature just below T_C in zero field and temperature just above T_C in field of 5 T. The parameters correspond to the fits shown in Fig. 7. The parameters for alloys that have been driven to a FM state by reducing temperature in zero field are different from those of alloys of the same chemical composition that have been driven to a FM state by increasing magnetic field isothermally, indicating the presence of differences in their local structure.

Composition/ Magnetic temperature field	a (Å)	b (Å)	c (Å)	γ°
$\text{Gd}_5\text{Si}_{0.2}\text{Ge}_{3.8}$ 0 T 30 K	7.5427(9)	14.7676(1)	7.8066(9)	90.14(1)
$\text{Gd}_5\text{Si}_{0.2}\text{Ge}_{3.8}$ 5 T 55 K	7.5587(9)	14.7482(1)	7.8016(9)	90.19(1)
$\text{Gd}_5\text{Si}_{0.7}\text{Ge}_{3.3}$ 0 T 70 K	7.5751(9)	14.7477(1)	7.7601(9)	90.10(1)
$\text{Gd}_5\text{Si}_{0.7}\text{Ge}_{3.3}$ 5 T 95 K	7.5752(9)	14.7785(16)	7.7666(9)	90.13(1)
$\text{Gd}_5\text{Si}_{1.7}\text{Ge}_{2.3}$ 0 T 205 K	7.5564(9)	14.7049(16)	7.7581(9)	90.240(2)
$\text{Gd}_5\text{Si}_{1.7}\text{Ge}_{2.3}$ 5 T 230 K	7.5546(9)	14.7307(16)	7.7715(9)	89.780(2)

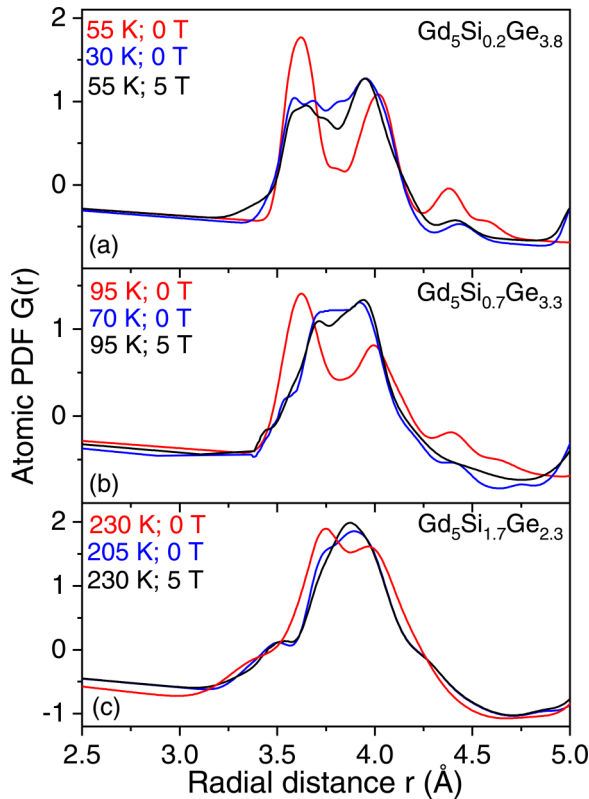


FIG. 9. Distribution of first neighbor Gd-Gd distances in $\text{Gd}_5\text{Si}_x\text{Ge}_{4-x}$ alloys extracted from the PDF fits shown in Fig. 7. The distribution for Ge-rich alloys (a),(b) in PM state is characteristic to the Gd_5Ge_4 -type structure and that for the intermediate alloy (c) is characteristic to the Gd_5Si_4 -type structure [compare with data in Fig. 2(a)]. The distribution appears smeared in the FM state due to the emergence of significant local structural distortions that reduce the crystallographic symmetry from orthorhombic to monoclinic. Data for PM alloys are given as red line. Data for FM alloys obtained by either decreasing temperature in zero field or increasing magnetic field isothermally are given as a blue and black line, respectively.

IV. DISCUSSION

For Heisenberg-type ferromagnets where the single ion anisotropy of magnetic species is negligible and magnetic interactions are of an oscillatory RKKY type, such as $\text{Gd}_5\text{Si}_x\text{Ge}_{4-x}$ alloys [33], the strength of magnetic exchange coupling depends strongly on the mutual coordination of nearby magnetic species [34,35]. Regardless of how the PM-to-FM transition is induced, a marked repositioning of Gd-Gd near neighbors in the alloys takes place, as revealed by the experimental PDFs in Fig. 6 and computed distribution of Gd-Gd pair distances shown in Fig. 9. Largely, it involves near neighbor Gd atoms from adjacent slabs, which slide with respect to one another, as shown in Fig. 10. In particular, in the higher temperature PM state (Fig. 10 left), slabs in $\text{Gd}_5\text{Si}_x\text{Ge}_{4-x}$ alloys ($0 < x \leq 2$) are largely arranged in a manner characteristic of Gd_5Ge_4 [compare green bars in Fig. 2(a) and red curves in Fig. 9]. At low temperature, this configuration is known to favor ferromagnetic interaction between Gd atoms in the slabs and antiferromagnetic

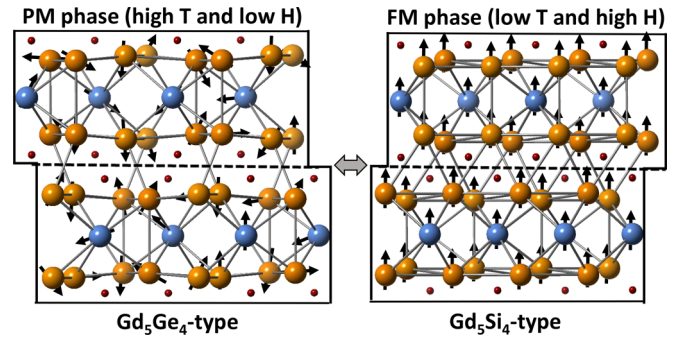


FIG. 10. Stacking of Gd-(Ge/Si) slabs in the high temperature PM (left) and low temperature FM (right) phases of studied $\text{Gd}_5\text{Si}_x\text{Ge}_{4-x}$ alloys, where the slabs can reversibly slide with respect to one another (broken line) at a particular low temperature or high magnetic field. The stacking is characteristic to the end members Gd_5Ge_4 (left) and Gd_5Si_4 (right), respectively. Nonmetal atoms positioned between the slabs are shown as red circles. For both phases, Gd atoms in the slabs (blue circles) have the same Gd-Gd coordination within 4 Å, where all first Gd neighbors are positioned in the slab. For Gd atoms at the slab sides (brown circles), some of the first Gd neighbors are from an adjacent slab, rendering Gd-Gd coordination and exchange coupling between the slabs in the PM (Gd_5Ge_4 -like) and FM (Gd_5Si_4 -like) phases different. The observed evolution of peaks in the experimental PDFs shown in Fig. 6 largely reflects changes in the mutual arrangement of near-neighbor Gd atoms from adjacent slabs induced by either decreasing temperature or increasing magnetic field. Distances between first neighbor Gd atoms positioned at least 4 Å apart are given as gray lines and spins of Gd atoms are given as short black arrows. The shift of the slabs shown here is up to scale.

interactions between Gd atoms from adjacent slabs, that is, when the alloys are cooled down to T_C , spins of Gd atoms in the constituent slabs would increasingly appear ferromagnetically ordered while those of Gd atoms in adjacent slabs would not. Then, the metamagnetic PM-to-FM phase transition in these alloys can be rationalized as follows: when strong magnetic field is applied at a temperature just above T_C , spins of all Gd atoms in the alloys would be pushed to align in a ferromagnetic ordering pattern, causing the slabs to slide with respect to one another so that the more closely packed, “ferromagnetic” stacking sequence of slabs characteristic to Gd_5Si_4 alloy (Fig. 10 right) is achieved. The sliding would be facilitated by the presence of distinct Si and Ge species in the space between the slabs and related local structural disorder, which, in turn, is inherited by the emerging ferromagnetic phase reducing its local symmetry to monoclinic (see the significantly smeared distribution of Gd-Gd distances in FM alloys given as blue and black curves in Fig. 9). Concurrently, the unit cell volume would drop (see Fig. 5) and X-X dimers form, which could enhance further the FM slab-slab interactions [8]. Notably, in this model picture, the formation of dimers appears as an artifact and not a driving force of the metamagnetic phase transition induced by the application of strong magnetic field.

For the pressure induced PM-to-FM transition, the following reasoning may apply. As can be seen in Figs. 1(c)

and 2(c), T_C increases markedly with Si content. The increase is consistent with the decrease in unit cell volume due to the smaller size of Si atoms in comparison to Ge atoms. Thus, applying pressure above T_C is, in a way, equivalent to replacing larger Ge atoms by smaller Si atoms, which destabilizes the higher volume PM phase, transforming it to a smaller volume phase (see the marked volume drop at T_C in Fig. 5), inevitably including sliding of Gd-X slabs with respect to one another and related emergence of FM order.

Last, decreasing temperature at constant pressure and zero magnetic field causes shrinking of all interatomic distances, which would destabilize the higher volume PM phase and induce a coupled structural and magnetic phase transition, where Gd-X slabs would slide against one another to adopt a smaller volume, FM phase. The resulting repositioning of spins of near neighbor Gd atoms from adjacent Gd-X slabs thus appears to be the salient feature of the observed first order PM-to-FM transition, be it induced by decreasing temperature, increasing pressure, or applying strong magnetic field. Notably, although, on average, the crystal structure of FM phases induced by different external stimuli appears the same, locally, the atomic arrangement in the phases is not necessarily the same (see the respective lattice parameters in Table I). Evidently, different external stimuli may render the alloys traverse the PM/FM phase boundary following different trajectories of local structure changes, opening a possibility to explore nontrivial FM phase states in search of improved magnetoresistance and magnetocaloric properties.

V. SUMMARY

Our variable temperature and magnetic fields study reveals features of the first order PM-to-FM transition in $Gd_5Si_xGe_{4-x}$ alloys ($0 < x \leq 2$) that remained not well appreciated by traditional crystallographic techniques. In particular, it reveals that, besides the concomitant formation of Si/Ge-Si/Ge dimers, the transition involves a marked repositioning of near neighbor Gd atoms from adjacent Gd-Si/Ge slabs leading to the emergence of ferromagnetic slab-slab interactions at low temperature and in strong magnetic field, and it is likely this repositioning that strongly couples the spin and lattice degrees of freedom in the alloys. Our work clarifies on the interaction between spin and lattice degrees of freedom in systems where spin-orbit coupling is negligible, in particular Gd-based systems that are difficult to study by neutron diffraction, demonstrating the great potential of *in situ* x-ray PDF analysis in magnetic field.

ACKNOWLEDGMENTS

This work was supported by the U.S. Department of Energy, Office of Science, Office of Basic Energy Sciences under Award No. DE-SC0021973 and used resources of the National Synchrotron Light Source at the Brookhaven National Laboratory provided by the DOE Office of Science under Contract No. DE-SC0012704. A portion of this work was performed at the National High Magnetic Field Laboratory, which is supported by the National Science Foundation Cooperative Agreement No. DMR-1644779 and the State of Florida.

-
- [1] Z. Hou, L. Li, Ch. Liu, X. Gao, X. Zhang, Zh. Ma, G. Zhou, Y. Peng, M. Yan, Xi-x. Zhang, and J. Liu, *Mater. Today Phys.* **17**, 100341 (2021).
 - [2] W. Ma, X. Xu, J.-X. Yin, H. Yang, H. Zhou, Z.-J. Cheng, Y. Huang, Z. Qu, F. Wang, M. Z. Hasan, and S. Jia, *Phys. Rev. Lett.* **126**, 246602 (2021).
 - [3] C. Gao, Z. Zeng, S. Peng, and C. Shuai, *Bioact. Mater.* **8**, 177 (2022).
 - [4] S. Zuo, J. Liu, K. Qiao, Y. Zhang, J. Chen, N. Su, Y. Liu, J. Cao, T. Zhao, J. Wang, F. Hu, J. Sun, C. Jiang, and B. Shen, *Adv. Mater.* **33**, 2103751 (2021).
 - [5] C. Bhandari, M. E. Flatté, and D. Paudyal, *Phys. Rev. Mater.* **5**, 094415 (2021).
 - [6] V. K. Pecharsky and K. A. Gschneider Jr., *Adv. Mater.* **13**, 683 (2001).
 - [7] A. Giguere, M. Foldeali, B. R. Gopal, R. Chahine, T. K. Bose, A. Frydman, and J. A. Barclay, *Phys. Rev. Lett.* **83**, 2262 (1999).
 - [8] W. Choe, V. K. Pecharsky, A. O. Pecharsky, K. A. Gschneider, Jr., V. G. Yong, and G. J. Miller, *Phys. Rev. Lett.* **84**, 4617 (2000).
 - [9] Z. W. Ouyang, V. K. Pecharsky, K. A. Gschneider, Jr., D. L. Schlageel, and T. A. Lograsso, *Phys. Rev. B* **74**, 094404 (2006).
 - [10] E. M. Levin, K. A. Gschneider, Jr., and V. K. Pecharsky, *Phys. Rev. B* **65**, 214427 (2002).
 - [11] J. E. Iglesias and H. Steinfink, *J. Less-Comm. Met.* **26**, 45 (1972).
 - [12] F. Holtzberg, R. J. Gambino, and T. R. McGuire, *J. Phys. Chem. Solids* **28**, 2283 (1967).
 - [13] V. K. Pecharsky and K. A. Gschneider, Jr., *Pure. Appl. Chem.* **79**, 1383 (2007).
 - [14] D. Haskel, Y. B. Lee, B. N. Harmon, Z. Islam, J. C. Lang, G. Srajer, Ya. Mudryk, K. A. Gschneider, Jr., and V. K. Pecharsky, *Phys. Rev. Lett.* **98**, 247205 (2007).
 - [15] L. Morellon, J. Blasco, P. A. Algarabel, and M. R. Ibarra, *Phys. Rev. B* **62**, 1022 (2000).
 - [16] C. Magen, Z. Arnold, L. Morellon, Y. Skorokhod, P. A. Algarabel, M. R. Ibarra, and J. Kamarad, *Phys. Rev. Lett.* **91**, 207202 (2003).
 - [17] L. Morellon, P. A. Algarabel, M. R. Ibarra, J. Blasco, B. Garcia-Landa, Z. Arnold, and F. Albertini, *Phys. Rev. B* **58**, R14721(R) (1998).
 - [18] Ya. Mudryk, Y. Lee, T. Vogt, K. A. Gschneider, Jr., and V. K. Pecharsky, *Phys. Rev. B* **71**, 174104 (2005).
 - [19] W. Choe, G. J. Miller, S. Chumbley, and A. O. Pecharsky, *Chem. Mater.* **15**, 1413 (2003).
 - [20] V. Franco, J. S. Blázquez, B. Ingale, and A. Conde, *Annu. Rev. Mater. Res.* **42**, 305 (2012).
 - [21] G. Scorek, J. Denisszczyk, and J. Szade, *J. Phys.: Condens. Matter* **14**, 7273 (2002).
 - [22] J. Szade and O. Skorek, *J. Magn. Magn. Mater.* **196**, 699 (1999).

- [23] K. H. J. Buschow, *J. Less-Comm. Met.* **43**, 55 (1975).
- [24] A. T. Hindmarch and B. J. Hickey, *Phys. Rev. Lett.* **91**, 116601 (2003).
- [25] C. L. Farrow, P. Juhás, J. W. Liu, D. Bryndin, E. S. Božin, J. Bloch, Th. Proffen, and S. J. L. Billinge, *J. Phys.: Condens. Matter* **19**, 335219 (2007).
- [26] B. H. Toby and R. B. Von Dreele, *J. Appl. Crystallogr.* **46**, 544 (2013).
- [27] V. Petkov, *Mater. Today* **11**, 28 (2008).
- [28] T. Egami and S. J. L. Billinge, in *Underneath the Braggs' Peaks* (Pergamon, Amsterdam, 2003).
- [29] See Supplemental Material at <http://link.aps.org/supplemental/10.1103/PhysRevMaterials.6.104407> for atomic PDFs and results from their analysis.
- [30] P. Juhás, T. Davis, C. L. Farrow, and S. J. L. Billinge, *J. Appl. Crystallogr.* **46**, 560 (2013).
- [31] G. L. Liu, J. R. Sun, J. Lin, Y. W. Xie, T. Y. Zhao, H. W. Zhang, and B. G. Shen, *Appl. Phys. Lett.* **88**, 212505 (2006).
- [32] E. M. Levin, A. O. Pecharsky, V. K. Pecharsky, and K. A. Gschneidner Jr, *Phys. Rev. B* **63**, 064426 (2001).
- [33] R. Skomski and D. J. Sellmyer, *J. Rare Earths* **27**, 675 (2009).
- [34] G. S. Rushbrooke and P. J. Wood, *Mol. Phys.* **1**, 257 (1958).
- [35] A. Hernando, J. M. Rojo, J. C. Gomez Sal, and J. M. Novo, *J. Appl. Phys.* **79**, 4815 (1996).